

**The  $^{92}\text{Zr}(n, \gamma)$  reaction and its implications for stellar nucleosynthesis**

G. Tagliente,<sup>1,2,\*</sup> P. M. Milazzo,<sup>3</sup> K. Fujii,<sup>3</sup> U. Abbondanno,<sup>3</sup> G. Aerts,<sup>4</sup> H. Álvarez,<sup>5</sup> F. Alvarez-Velarde,<sup>6</sup> S. Andriamonje,<sup>4</sup> J. Andrzejewski,<sup>7</sup> L. Audouin,<sup>8</sup> G. Badurek,<sup>9</sup> P. Baumann,<sup>10</sup> F. Bečvář,<sup>11</sup> F. Belloni,<sup>3</sup> E. Berthoumieux,<sup>4</sup> S. Bisterzo,<sup>12</sup> F. Calviño,<sup>13</sup> M. Calviani,<sup>14</sup> D. Cano-Ott,<sup>6</sup> R. Capote,<sup>15,16</sup> C. Carrapiço,<sup>17</sup> P. Cennini,<sup>18</sup> V. Chepel,<sup>19</sup> E. Chiaveri,<sup>18</sup> N. Colonna,<sup>1</sup> G. Cortes,<sup>13</sup> A. Couture,<sup>20</sup> J. Cox,<sup>20</sup> M. Dahlfors,<sup>18</sup> S. David,<sup>10</sup> I. Dillmann,<sup>8</sup> C. Domingo-Pardo,<sup>21</sup> W. Dridi,<sup>4</sup> I. Duran,<sup>5</sup> C. Eleftheriadis,<sup>22</sup> M. Embid-Segura,<sup>6</sup> A. Ferrari,<sup>18</sup> R. Ferreira-Marques,<sup>19</sup> W. Furman,<sup>23</sup> R. Gallino,<sup>12</sup> I. Goncalves,<sup>19</sup> E. Gonzalez-Romero,<sup>6</sup> F. Gramegna,<sup>14</sup> C. Guerrero,<sup>6</sup> F. Gunsing,<sup>4</sup> B. Haas,<sup>24</sup> R. Haight,<sup>25</sup> M. Heil,<sup>8</sup> A. Herrera-Martinez,<sup>18</sup> M. Igashira,<sup>26</sup> E. Jericha,<sup>9</sup> F. Käppeler,<sup>8</sup> Y. Kadi,<sup>18</sup> D. Karadimos,<sup>27</sup> D. Karamanis,<sup>27</sup> M. Kerveno,<sup>10</sup> E. Kossionides,<sup>28</sup> M. Krtička,<sup>11</sup> C. Lamboudis,<sup>22</sup> H. Leeb,<sup>9</sup> A. Lindote,<sup>19</sup> I. Lopes,<sup>19</sup> M. Lozano,<sup>16</sup> S. Lukic,<sup>10</sup> J. Marganec,<sup>7</sup> S. Marrone,<sup>1</sup> T. Martínez,<sup>6</sup> C. Massimi,<sup>29</sup> P. Mastinu,<sup>14</sup> A. Mengoni,<sup>15</sup> C. Moreau,<sup>3</sup> M. Mosconi,<sup>8</sup> F. Neves,<sup>19</sup> H. Oberhummer,<sup>9</sup> S. O'Brien,<sup>20</sup> J. Pancin,<sup>4</sup> C. Papachristodoulou,<sup>27</sup> C. Papadopoulos,<sup>30</sup> C. Paradela,<sup>5</sup> N. Patronis,<sup>27</sup> A. Pavlik,<sup>31</sup> P. Pavlopoulos,<sup>32</sup> L. Perrot,<sup>4</sup> M. T. Pigni,<sup>9</sup> R. Plag,<sup>8</sup> A. Plompen,<sup>33</sup> A. Plukis,<sup>4</sup> A. Poch,<sup>13</sup> J. Praena,<sup>14</sup> C. Pretel,<sup>13</sup> J. Quesada,<sup>16</sup> T. Rauscher,<sup>34</sup> R. Reifarth,<sup>25</sup> M. Rosetti,<sup>35</sup> C. Rubbia,<sup>36</sup> G. Rudolf,<sup>10</sup> P. Rullhusen,<sup>33</sup> J. Salgado,<sup>17</sup> C. Santos,<sup>17</sup> L. Sarchiapone,<sup>18</sup> I. Savvidis,<sup>22</sup> C. Stephan,<sup>37</sup> J. L. Tain,<sup>21</sup> L. Tassan-Got,<sup>37</sup> L. Tavora,<sup>17</sup> R. Terlizzi,<sup>1</sup> G. Vannini,<sup>29</sup> P. Vaz,<sup>17</sup> A. Ventura,<sup>35</sup> D. Villamarin,<sup>6</sup> M. C. Vicente,<sup>6</sup> V. Vlachoudis,<sup>18</sup> R. Vlastou,<sup>30</sup> F. Voss,<sup>8</sup> S. Walter,<sup>8</sup> H. Wendler,<sup>18</sup> M. Wiescher,<sup>20</sup> and K. Wisshak<sup>8</sup>  
(n.TOF Collaboration<sup>†</sup>)

<sup>1</sup>*Istituto Nazionale di Fisica Nucleare (INFN), Bari, Italy*

<sup>2</sup>*University of Ghent, Ghent, Belgium*

<sup>3</sup>*Istituto Nazionale di Fisica Nucleare (INFN), Trieste, Italy*

<sup>4</sup>*CEA/Saclay-IRFU, Gif-sur-Yvette, France*

<sup>5</sup>*Universidad de Santiago de Compostela, Santiago de Compostela, Galicia, Spain*

<sup>6</sup>*Centro de Investigaciones Energeticas Medioambientales y Technologicas, Madrid, Spain*

<sup>7</sup>*University of Lodz, Lodz, Poland*

<sup>8</sup>*Forschungszentrum Karlsruhe GmbH (FZK), Institut für Kernphysik, Karlsruhe, Germany*

<sup>9</sup>*Atominstytut der Österreichischen Universitäten, Technische Universität Wien, Wien, Austria*

<sup>10</sup>*Centre National de la Recherche Scientifique/IN2P3-IRES, Strasbourg, France*

<sup>11</sup>*Faculty of Mathematics and Physics, Charles University, Prague, Czech Republic*

<sup>12</sup>*Dipartimento di Fisica Generale, Università di Torino, Torino, Italy*

<sup>13</sup>*Universitat Politècnica de Catalunya, Barcelona, Spain*

<sup>14</sup>*Istituto Nazionale di Fisica Nucleare (INFN), Laboratori Nazionali di Legnaro, Legnaro, Italy*

<sup>15</sup>*International Atomic Energy Agency (IAEA), NAPC/Nuclear Data Section, Vienna, Austria*

<sup>16</sup>*Universidad de Sevilla, Sevilla, Spain*

<sup>17</sup>*Instituto Tecnológico e Nuclear (ITN), Lisbon, Portugal*

<sup>18</sup>*CERN, Geneva, Switzerland*

<sup>19</sup>*LIP-Coimbra & Departamento de Física da Universidade de Coimbra, Coimbra, Portugal*

<sup>20</sup>*University of Notre Dame, South Bend, Indiana 46556, USA*

<sup>21</sup>*Instituto de Física Corpuscular, CSIC-Universidad de Valencia, Valencia, Spain*

<sup>22</sup>*Aristotle University of Thessaloniki, Thessaloniki, Greece*

<sup>23</sup>*Joint Institute for Nuclear Research, Frank Laboratory of Neutron Physics, Dubna, Russia*

<sup>24</sup>*Centre National de la Recherche Scientifique/IN2P3-CENBG, Bordeaux, France*

<sup>25</sup>*Los Alamos National Laboratory, Los Alamos, New Mexico 87545, USA*

<sup>26</sup>*Tokyo Institute of Technology, Tokyo, Japan*

<sup>27</sup>*University of Ioannina, Ioannina, Greece*

<sup>28</sup>*NCSR, Athens, Greece*

<sup>29</sup>*Dipartimento di Fisica, Università di Bologna, and Sezione INFN di Bologna, Bologna, Italy*

<sup>30</sup>*National Technical University of Athens, Athens, Greece*

<sup>31</sup>*Institut für Fakultät für Physik, Universität Wien, Wien, Austria*

<sup>32</sup>*Pôle Universitaire Léonard de Vinci, Paris La Défense, Paris, France*

<sup>33</sup>*CEC-JRC-IRMM, Geel, Belgium*

<sup>34</sup>*Department of Physics and Astronomy, University of Basel, Basel, Switzerland*

<sup>35</sup>*ENEA, Bologna, Italy*

<sup>36</sup>*Università degli Studi di Pavia, Pavia, Italy*

<sup>37</sup>*Centre National de la Recherche Scientifique/IN2P3-IPN, Orsay, France*

(Received 22 April 2009; revised manuscript received 26 February 2010; published 5 May 2010)

Because the relatively small neutron capture cross sections of the zirconium isotopes are difficult to measure, the results of previous measurements are often not adequate for a number of problems in astrophysics and nuclear

technology. Therefore, the  $^{92}\text{Zr}(n,\gamma)$  cross section has been remeasured at the CERN n.TOF facility, providing a set of improved parameters for 44 resonances in the neutron energy range up to 40 keV. With this information the cross-section uncertainties in the keV region could be reduced to 5% as required for *s*-process nucleosynthesis studies and technological applications.

DOI: 10.1103/PhysRevC.81.055801

PACS number(s): 25.40.Lw, 25.70.Ef, 27.60.+j, 28.41.Qb

## I. INTRODUCTION

Stellar nucleosynthesis of heavy elements [1,2] is characterized by two dominant neutron capture processes, which differ by their respective time scales. The *r* (rapid) process is related to extremely hot, neutron-rich environments ( $T > 10^9$  K,  $n_n \gg 10^{20}$  cm $^{-3}$ ) and occurs presumably in supernova explosions, whereas the *s* (slow) process operates during the He burning stages of stellar evolution at lower temperatures and neutron densities ( $T \approx 10^8$  K,  $n_n \approx 10^8$  cm $^{-3}$ ). Correspondingly, the notation slow and rapid refers to the comparison with average  $\beta$ -decay lifetimes.

Accurate *s*-process analyses have attracted great interest, thanks to the progress in astronomical observations and stellar modeling [3]. The understanding of the *s*-process has advanced from a phenomenological description of the abundance distribution in the solar system toward a comprehensive picture, which includes the overall aspects of stellar and galactic evolution. Owing to this development, the *s* process could be established as an important way to probe the evolution of Red Giant stars.

The success of the stellar *s*-process models depends to a large extent on significant improvements in the neutron capture cross-section data. An accuracy of only a few percent, which can be reached with modern techniques, turned out to be a prerequisite for detailed studies of the physical conditions during stellar He burning. However, the uncertainties of many cross-section data must still be improved to the required level of accuracy, particularly in the mass region  $A \leq 100$  as well as for nuclei with small and resonance-dominated cross sections [4].

The comparably small cross sections of the Zr isotopes represent an important example of this situation. They are predominantly of *s*-process origin and belong to the first *s*-process peak in the solar abundance distribution around  $A \approx 90$ . Because the flow equilibrium was partly established in the *s*-process reaction chain, the resulting isotopic abundances are determined by the stellar neutron capture rate, that is, by the neutron capture cross section  $\sigma(E_n)$  integrated over the stellar spectrum. The stellar neutron flux corresponds to a Maxwell-Boltzmann distribution [4], because neutrons are quickly thermalized in the dense He burning plasma, and the effective stellar cross sections for *s*-process studies can be expressed as Maxwellian-averaged capture cross sections (MACSs) [5].

The astrophysical importance of an improved MACS for  $^{92}\text{Zr}$  at stellar energies is related to the overabundance of  $^{92}\text{Zr}$  reported in Ref. [6]. Using the previously recommended MACS values [4], it was calculated that 93% of solar  $^{92}\text{Zr}$  was of *s*-process origin, notwithstanding the expected *r*-process contribution of 10% inferred from the neighboring isotopes.

Therefore, the MACS value of  $^{92}\text{Zr}$  needs to be verified to refine the constraints for the *s*-process models and to study the consequences for the *r*-process component. A better determination of the solar  $^{92}\text{Zr}$  production is also related to the potential interpretation of the  $^{92}\text{Nb}/^{92}\text{Zr}$  pair as a cosmochronometer [7] for the early solar system.

For nuclear technology the transmutation of the long-lived fission products (LLFPs)  $^{79}\text{Se}$ ,  $^{93}\text{Zr}$ ,  $^{99}\text{Tc}$ ,  $^{107}\text{Pd}$ ,  $^{126}\text{Sn}$ ,  $^{129}\text{I}$ , and  $^{135}\text{Cs}$  by neutron capture is of great interest. While direct information on the capture cross sections of LLFPs is indispensable for studies of possible transmutation systems, these data are also needed for the respective stable isotopes, because these are coproduced by fission and accompany the LLFPs in the transmutation process unless the LLFPs are isotopically separated. Moreover, the samples used in cross-section measurements of LLFPs are ordinarily prepared from fission products by radiochemical techniques. Such a sample for a capture measurement of the  $^{93}\text{Zr}$  cross section would contain only 20%  $^{93}\text{Zr}$ . Obviously, the corrections owing to the expected isotopic interferences can only be evaluated with accurate cross-section data for the stable Zr isotopes.

Existing experimental data mainly come from relatively old measurements [8–11]. Reference [9] lists the energies of the resonances up to 40 keV and gives capture kernels up to 10 keV (with associated errors of between 10% and 20%); Ref. [10] lists some resonances (15 of 52 known in this range) up to 52 keV but gives detailed information only for four strong resonances. Reference [11] lists five resonances, but the first one has been recognized as not belonging to  $^{92}\text{Zr}$ . A recent publication [12] does not present the resonance analysis. The only rich information available is that present in the mid-1970 publication [8], already revisited by evaluators [13,14].

In view of this situation the cross sections of the Zr isotopes have been remeasured at the n.TOF facility at CERN using specifically designed experimental techniques and analysis tools [15,16]. The experimental details are presented in Sec. II, followed by the determination of capture yields (Sec. III) and backgrounds (Sec. IV). The resonance analysis is discussed in Sec. V, and the results are compared with previous measurements in Sec. VI. The implications of present measurements for stellar nucleosynthesis are briefly discussed in Sec. VII.

## II. EXPERIMENTAL SETUP

### A. Characteristics of the neutron beam

At the CERN n.TOF facility neutrons in a wide energy range, from thermal to more than 250 MeV, are produced by spallation reactions induced by proton bunches of high energy (20 GeV), high intensity ( $7 \times 10^{12}$  protons per bunch), short width ( $\Delta t = 6$  ns), and low duty factor (repetition rates of 0.4 to 0.8 Hz) in a massive lead target. The spallation

\* giuseppe.tagliente@ba.infn.it

† URL: www.cern.ch/ntof

neutrons are moderated in the lead target and in a 5.8-cm-thick layer of cooling water surrounding the target. The moderation process produces a nearly  $1/E$  isoethargic flux up to 1 MeV. The neutron beam is transported through an evacuated flight path with collimators at 135 and 175 m to the measuring station at a distance of 185.2 m from the spallation target. The beam line extends 12 m beyond the experimental area to minimize the effect of back-scattered neutrons. Background owing to fast-charged particles is suppressed by a 1.5-T sweeping magnet, heavy concrete walls, and a 3.5-m-thick iron shielding [17].

The features of the n\_TOF facility, in particular, the high instantaneous neutron flux ( $10^5$  neutrons/cm<sup>2</sup>/pulse at the measuring position), high resolution ( $3 \times 10^{-4}$  at 1 eV,  $1.5 \times 10^{-3}$  at 30 keV), and low background allow one to collect capture cross-section data with good accuracy and an excellent signal-to-background ratio and provide the possibility for improved measurement of the small capture cross section of  $^{92}\text{Zr}$  in the energy range between 1 eV and 1 MeV.

The relative neutron flux was measured with a low-mass flux monitor consisting of a Mylar foil 1.5  $\mu\text{m}$  thick with a layer of 200  $\mu\text{g}/\text{cm}^2$   $^6\text{Li}$ . Charged particles emitted in  $^6\text{Li}(n,\alpha)^3\text{H}$  reactions were detected by a set of four Si detectors surrounding the  $^6\text{Li}$  sample outside the neutron beam [18]. The monitor sample was located 1.5 m upstream of the capture samples. The neutron beam was also periodically checked by calibration runs with gold reference samples.

### B. Capture detectors

Two  $\text{C}_6\text{D}_6$  liquid scintillator cells were used to detect the prompt  $\gamma$ -ray cascade following neutron capture. The detectors were mounted perpendicular to the neutron beam at a distance of about 3 cm from the beam axis. Background owing to in-beam  $\gamma$ -rays from  $(n,\gamma)$  reactions in the water moderator [17] was reduced by placing the detectors 9.2 cm upstream of the sample position.

The detectors were optimized with respect to background induced by neutrons scattered from the sample, which are captured in the detectors or in nearby parts of the experimental setup [19]. The scintillator cells consisted of thin Kapton-coated carbon-fiber cylinders, which were directly glued onto EMI-9823QKB photomultiplier tubes. Compared to the commercial detector type, the neutron sensitivity could be reduced by an order of magnitude, an important advantage for measurements on isotopes with high scattering/capture ratios.

Details of the detectors and the experimental setup can be found elsewhere [20]. The detectors were calibrated in regular intervals by means of  $^{137}\text{Cs}$  (662-keV) and  $^{60}\text{Co}$  (1173- and 1332-keV) reference sources. An additional calibration point at 6.13 MeV was obtained with a composite  $^{238}\text{Pu}/^{13}\text{C}$  source.

Detector signals were recorded with fast digitizers with a sampling rate of 500 Msamples/s and an onboard memory of 8 Mbyte. In this way, each neutron burst was followed for 16 ms, corresponding to a minimum neutron energy of 0.7 eV. Data were processed between successive bursts by the standard n\_TOF data acquisition system [21].

TABLE I. Characteristics of the  $^{92}\text{Zr}$  sample.

Sample	Chemical form	Isotope composition (%)				
		$^{90}\text{Zr}$	$^{91}\text{Zr}$	$^{92}\text{Zr}$	$^{94}\text{Zr}$	$^{96}\text{Zr}$
$^{92}\text{Zr}$	$\text{ZrO}_2$	4.65	1.62	91.4	2.03	0.30

### C. Samples

The  $^{92}\text{Zr}$  sample was prepared from  $\text{ZrO}_2$  powder, which was pressed into a pellet 22 mm in diameter, 0.07 cm thick, and 1.349 g in mass and encapsulated in a 0.2-mm-thick aluminum can. The sample was enriched to 91.4% in  $^{92}\text{Zr}$  but contained small amounts of all stable Zr isotopes as well (Table I). Traces of Hf, Sn, Na, Mg, and Al were also present in the sample. The contribution of these impurities to the measured capture yield was not negligible and had to be considered in data analysis.

Additional C, Au, and Pb samples of the same diameter were used for repeated neutron flux measurements and background runs throughout the experiment. These samples were made from metal of natural composition. The relevant sample characteristics are summarized in Table I.

## III. DETERMINATION OF CAPTURE YIELDS

The capture yield  $Y(E_n)$ , which is defined as the fraction of incident neutrons of energy  $E_n$  undergoing  $(n,\gamma)$  reactions in the measured sample, is directly related to the capture and total cross sections. The liquid scintillator detectors have a low efficiency and cover a restricted solid angle far below  $4\pi$ , resulting in an overall efficiency for the detection of capture events of  $\approx 20\%$ . Because the efficiency for capture events depends in a complex way on the emitted  $\gamma$ -ray spectrum, the absolute yield has been determined via the pulse height weighting technique (PHWT) and by normalization to the standard cross section of a reference isotope.

The PHWT is based on the off-line modification of the response function of the detector in such a way that the efficiency for capture cascades becomes proportional to the total  $\gamma$ -ray energy released in the event, independent of cascade multiplicity and the spectral shape of the  $\gamma$  spectrum [22–24]. The normalization to a reference cross section was performed by means of the saturated resonance technique [25] using the prominent 4.9-eV resonance in  $^{197}\text{Au}$ .

The neutron flux at n\_TOF has been measured with a  $^{235}\text{U}$ -loaded parallel-plate fission chamber from PTB Braunschweig [26] (see also Fig. 2 in Ref. [27]) as well as with the  $^6\text{Li}$  neutron flux monitors used during the experimental runs [18]. Additional flux measurements were performed by analysis of standard resonances [28]. Overall, the neutron flux could be determined with an uncertainty of 2%.

## IV. BACKGROUNDS

In view of the relatively small capture cross section of  $^{92}\text{Zr}$ , it is important to determine the different background components with a good accuracy. Relevant sources of background in this experiment were (a) neutrons scattered in

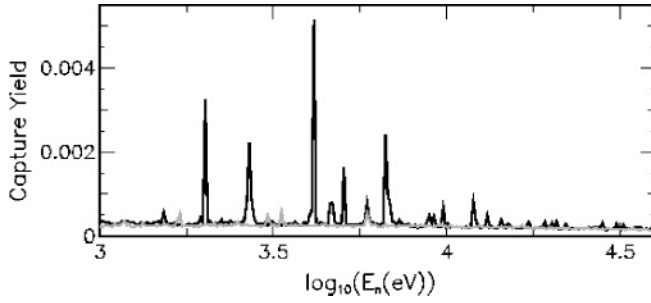


FIG. 1. Capture yield (black) and overall background (gray) in the investigated energy range ( $1 \text{ keV} < E_n < 40 \text{ keV}$ ).

the sample and captured in the detectors or in nearby parts of the experimental setup, (b) capture events in the aluminum can of the Zr sample, (c) in-beam  $\gamma$ -rays produced in the spallation target, and (d) the ambient background in the experimental area. Each of these sources is detailed here.

- (i) This contribution to the background was evaluated by means of a carbon sample, which can be considered a pure scatterer because the total cross section is dominated by the elastic channel. These dedicated runs showed that the effect of scattered neutrons was negligible in the spectra of  $^{92}\text{Zr}$ , owing to the very low neutron sensitivity of the setup [19,26].
- (ii) Measurements with an empty Al can showed that only a few well-known Al resonances were identifiable in the Zr spectra; this very small background component was easily subtracted.
- (iii) In-beam  $\gamma$  rays, which are produced mainly by neutron capture in the hydrogen of the water moderator and arrive at the sample together with keV-energy neutrons, are scattered from the sample and detected by the  $\text{C}_6\text{D}_6$  scintillators. This more severe background ( $\approx 70\%$  of total background) has been studied with a lead sample, because the high atomic number favors  $\gamma$  scattering, while  $(n, \gamma)$  reactions are strongly reduced by the low capture cross section.
- (iv) The correction for the comparably low ambient background was negligible.

The final capture yield and the overall background are presented in Fig. 1.

## V. RESONANCE ANALYSIS

The experimental capture yield,

$$Y^{\text{exp}} = \frac{Y_w}{N_n E_c} + B,$$

is determined by the weighted net count rate  $Y_w$ , the effective binding energy  $E_c$ , the integrated neutron flux  $N_n$ , and the overall background  $B$ . The weighted net count rate was normalized to the effective binding energy and to the integrated neutron flux.

The experimental capture yield has been analyzed in the Reich-Moore approximation with the multilevel  $\mathcal{R}$ -matrix program SAMMY [29]. Corrections for Doppler broadening

of resonance widths owing to thermal motions of the sample atoms, for energy resolution of the neutron beam and isotopic and chemical sample impurities, and for self-shielding and neutron multiple scattering are considered by the code. The effect of potential scattering was theoretically calculated using a radius of 7.2 fm [13].

The analysis was limited to the energy range between 2 and 40 keV because the statistical precision of the capture data was poor at higher energies. Among the 44 resonances analyzed, 3 resonances were identified for the first time.

For this isotope, the neutron widths  $\Gamma_n$  are much bigger than the radiative width  $\Gamma_\gamma$  for almost all resonances, so that the contribution of  $\Gamma_n$  to the capture kernel is negligible. Therefore  $\Gamma_n$  was kept fixed in the fit to the values reported in the literature [13,14], obtained from the transmission measurements in Ref. [8], for all resonances except the first one, for which  $\Gamma_\gamma$  was fixed instead. Similarly to  $\Gamma_n$ , in the present analysis the spin factors were fixed to the values reported in the evaluated library JENDL-3.3 [30], the capture data being insensitive to the resonance spin.

The deduced  $E_R$  (resonance energy) and  $\Gamma_\gamma$  resonance parameters are listed in Table II, together with the capture kernel:

$$K = g \frac{\Gamma_n \Gamma_\gamma}{(\Gamma_n + \Gamma_\gamma)},$$

where

$$g = \frac{(2J + 1)}{(2I_n + 1)(2I_{\text{Zr}} + 1)}$$

is the statistical spin factor determined by the resonance spin  $J$ , the spin of the incident neutron  $I_n = 1/2$ , and the spin of the target nucleus  $I_{\text{Zr}} = 0$ .

For the resonances observed in this work for the first time, only the capture kernel is reported, as an accurate resonance parameter would require a more refined combined analysis of capture and transmission data, which is outside the goal of the present paper.

Examples illustrating the quality of the fits are shown in Fig. 2.

Owing to the relatively low capture cross section of  $^{92}\text{Zr}$ , the overall uncertainties of the results are dominated by the counting statistics. The statistical uncertainty grows with the neutron energy, from  $\approx 4\%$  at 150 eV to  $\approx 6\%$  at 40 keV. Other sources of systematic uncertainty are the application of the PHWT, the energy dependence of the neutron flux, and the fraction of the neutron beam covered by the sample. The use of weighting functions obtained with different combinations of parameters and fit procedures confirmed that the related uncertainty is less than 2% [24]. Normalization of the neutron flux by means of the saturated resonance technique via the 4.9-eV resonance in  $^{197}\text{Au}$  also contributed an uncertainty of 2%.

## VI. COMPARISON WITH EXISTING DATA

The available experimental information on the  $^{92}\text{Zr}(n, \gamma)$  cross section is rather limited. The results from previous measurements either are old and incomplete [8–10] or reported

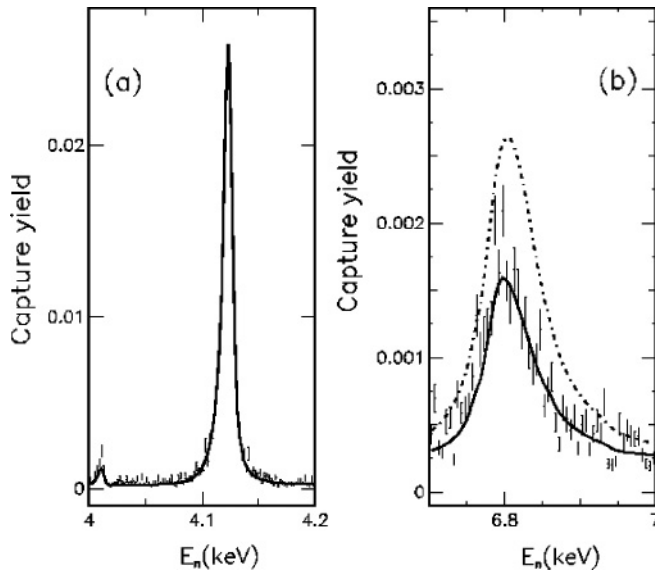


FIG. 2. Examples of fits with the  $\mathcal{R}$ -matrix code SAMMY (full lines). (a) The resonance at 4.2 keV, which turned out to be most important for calculation of the Maxwellian average. (b) The resonance at 6.8 keV, where the present results deviate significantly from the resonance parameters listed in Ref. [8] (dashed-dotted line).

the neutron capture cross section without resonance analysis [12]. The only information on resonance parameters comes from the work of Boldeman *et al.* [8], which was performed with a pair of nonhydrogenous fluorocarbon liquid scintillators [31] (capture measurement) and a  $^6\text{Li}$  glass scintillator (transmission measurement) at the Oak Ridge electron linac more than three decades ago.

The present  $\Gamma_\gamma$  values are 15% smaller compared to the results of Ref. [8] as shown in Fig. 3(a). This holds also for the capture kernels in Fig. 3(b), which are in first approximation proportional to  $\Gamma_\gamma$  because  $\Gamma_n \gg \Gamma_\gamma$  in almost all observed resonances.

The main reason for these observed differences resides in the neutron sensitivity. Previous data [8] were obtained with an experimental setup characterized by a non-negligible neutron sensitivity. In particular, Boldeman *et al.* used two detectors surrounded by a large amount of material, as shown in Fig. 2 of Ref. [31]. We remind the reader that the neutron sensitivity of the capture setup is particularly important in this measurement, considering the high scattering/capture ratio that characterizes  $^{92}\text{Zr}$ . In this respect, the measurement at n\_TOF is significantly more accurate than previous measurements, owing to the neutron sensitivity of the present setup. Further reasons for the differences could possibly be the more accurate determination of the weighting functions, the smaller influence of self-shielding and multiple scattering effects, the lower background, and the modern data acquisition techniques with fast digitizers, which allowed us to analyze the data off-line in the most flexible way, including an efficient pulse shape analysis for  $n/\gamma$  discrimination. Finally, a higher accuracy in the present data has been achieved thanks to the use of the well-tested and -documented  $R$ -matrix code [29].

TABLE II. Resonance parameters extracted from the fit of the n\_TOF capture data. Except for the first resonance, the values of  $\Gamma_n$  used in the SAMMY fit were kept fixed at values from Refs. [8], [13], and [14].

$E_R^a$ (eV)	$J$	$l$	$\Gamma_\gamma$ (eV)	$\Delta\Gamma_\gamma$ (%)	$\Gamma_n$ (eV)	$K$ (eV)	$\Delta K$ (%)
2 012.91(3) <sup>b</sup>	3/2	1	(0.36)	—	0.0260	0.0443	2.4
2 689.4(4)	1/2	0	0.115	1.8	25.	0.115	1.7
4 121.2(1)	3/2	1	0.250	1.4	3.	0.460	1.3
4 639.6(5)	1/2	0	0.100	3.1	15.	0.100	3.1
4 653.69(3) <sup>c</sup>	—	—	—	—	—	(0.0089)	(82.)
5 045.7(1)	1/2	1	0.165	2.7	1.	0.142	2.3
6 638.9(1)	3/2	1	0.224	2.4	1.	0.363	2.0
6 811.(3)	1/2	0	0.130	9.0	50.	0.132	9.0
8 845.0(4)	1/2	1	0.110	5.0	4.	0.107	4.8
9 136.7(5)	1/2	0	0.098	5.2	6.3	0.0970	5.2
9 821.0(3)	3/2	1	0.085	4.9	1.4	0.160	4.6
11 943.7(3)	3/2	1	0.130	4.4	1.6	0.240	4.1
12 013.1(7)	1/2	1	0.200	5.2	9.	0.195	5.1
13 065.7(4)	3/2	1	0.121	4.7	1.5	0.224	4.3
14 427.(1)	1/2	1	0.205	5.8	14.	0.202	5.7
15 027.9(8)	3/2	0	0.057	9.2	0.25	0.0980	8.0
16 941.0(1) <sup>c</sup>	—	—	—	—	—	(0.020)	(83.)
17 132.(1)	3/2	1	0.147	5.1	12.	0.290	5.1
17 284.6(1) <sup>c</sup>	—	—	—	—	—	(0.018)	(83.)
19 076.(1)	3/2	1	0.166	6.0	2.15	0.308	5.6
20 195.(1)	1/2	0	0.215	8.9	1.3	0.185	7.6
20 846.(1)	1/2	0	0.341	6.6	2.4	0.299	5.8
21 977.(1)	1/2	1	0.237	7.6	2.8	0.218	7.0
23 114(10)	1/2	0	0.150	9.5	108.	0.150	9.5
25 078.2(1)	—	—	—	—	—	(0.030)	(74.)
25 665.(4)	1/2	0	0.077	19.	2.5	0.0750	19.
26 236.(1)	—	—	—	—	—	(0.05)	(88.)
26 776.(3)	3/2	1	0.12	10.	1.15	0.22	9.5
27 327.(5)	1/2	1	0.20	12.	22.5	0.198	12.
28 098.(6)	3/2	1	0.068	20.	12.5	0.14	20.
28 167.(4)	1/2	1	0.28	13.	6.0	0.26	12.
28 282.(1)	—	—	—	—	—	(0.08)	(87.)
30 398.(7)	1/2	0	0.073	23.	4.6	0.072	23.
30 932.(3)	3/2	1	0.241	8.7	12.	0.473	8.5
32 490.(3)	3/2	1	0.310	7.5	11.5	0.604	7.3
33 094.(9)	1/2	0	0.10	11.	12.	0.10	11.
35 035(20)	1/2	1	0.290	6.6	65.	0.289	6.6
35 677(12)	1/2	1	0.417	8.0	52.	0.414	7.9
35 961.(7)	3/2	1	0.234	9.0	26.5	0.464	9.0
37 507.(7)	1/2	1	0.187	5.3	14.	0.185	5.2
38 740(10)	1/2	1	0.125	9.1	4.5	0.121	8.8
38 922(8)	3/2	1	0.10	11.	5.	0.20	11.
39 345(9)	1/2	1	0.44	14.	70.	0.44	14.
39 418(40)	1/2	0	0.12	14.	73.	0.12	14.

<sup>a</sup>Uncertainties are given as 2012.89(4)  $\equiv$  2012.89  $\pm$  0.04.

<sup>b</sup>The value of  $\Gamma_\gamma$  was fixed to literature values [13,14], while the value of  $\Gamma_n$  was fitted,  $\Gamma_n = 0.260 \pm 0.012$  eV (see text for details).

<sup>c</sup>New.

## VII. MAXWELLIAN AVERAGED CROSS SECTIONS

Zirconium plays an important role in the determination of the  $s$ -process abundances of heavy elements. The mass region around  $A = 90$ –100 is, in fact, particularly

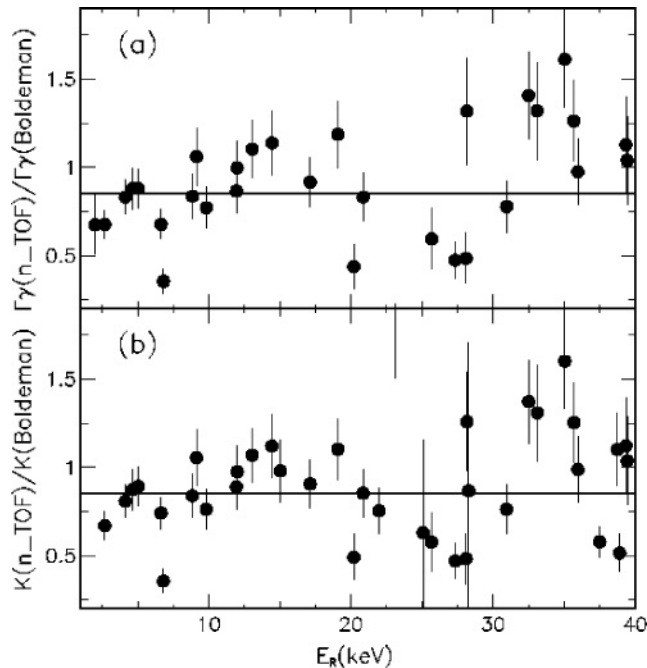


FIG. 3. (a) Ratio between  $\Gamma_\gamma$  values obtained in the present measurement and those given by Boldeman *et al.* [8] as a function of resonance energy. The average value is indicated by the solid horizontal line. (b) Ratio between capture kernels obtained in the present measurement and those given by Boldeman *et al.* [8].

interesting. Massive stars, where the  $s$  process takes place during the presupernova evolution, that is, during convective core helium burning and convective shell carbon burning [32], are responsible for the  $s$  abundances below  $A = 90$  but contribute very little to the heavier region. This so-called weak  $s$  process is complemented by the main  $s$  component in asymptotic giant branch (AGB) stars of  $1 \leq M/M_\odot \leq 3$  (where  $M_\odot$  denotes the mass of the Sun), which is producing the  $s$  abundances above  $A = 90$  [33,34]. Accordingly, Zr plays a key role in understanding the situation at the matching point of both components.

The MACSs, which are required for the quantitative description of the  $s$  abundances produced by the weak and main component [5], have been calculated by folding the capture cross section with the thermalized stellar spectra over a sufficiently wide neutron energy range, starting at about 100 eV and extending to about 500 keV at the highest temperatures reached during shell carbon burning in massive stars. A collection of MACSs for all isotopes along the  $s$  path is given in Ref. [4] and in the online database KADONIS [35].

In the following the MACS values are determined for three typical  $s$ -process situations: for the stellar environments in thermally pulsing, low-mass AGB stars at  $kT = 8$  and 23 keV, where neutrons are produced by  $(\alpha, n)$  reactions on  $^{13}\text{C}$  and  $^{22}\text{Ne}$ , respectively [33]; as well as for the standard thermal energy of  $kT = 30$  keV, which is commonly used for intercomparison.

For the resonance-dominated cross section of  $^{92}\text{Zr}$  the MACS is strongly dependent on the energy and strength of the most prominent resonances. This is illustrated in Fig. 4,

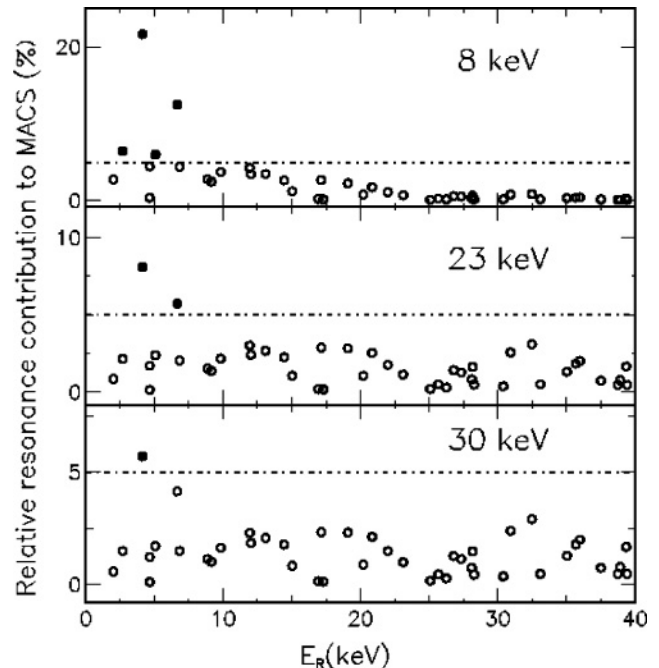


FIG. 4. Relative resonance contributions for the MACS at characteristic thermal energies. Resonances that contribute more than 5% to the MACS are indicated by filled circles.

where the relative resonance contributions are plotted for the characteristic thermal energies. The results of the present measurement cover the energy range up to 40 keV, which contributes 98%, 73%, and 64% of the MACS at 8, 23, and 30 keV, respectively. The comparison in Table III shows that the present capture kernels are 20% smaller on average than those reported in Ref. [8] (the relative contributions of these resonances illustrate their importance for the MACS at low thermal energies). This is most probably caused by the much lower neutron sensitivity of the n\_TOF experimental setup relative to those used in previous measurements [8,9]. The large improvement in the neutron sensitivity is particularly evident in the case of the 6.8-keV resonance, which is characterized by one of the highest  $\Gamma_n/\Gamma_\gamma$  ratios (Fig. 2). In this important case the present capture kernel is almost a factor of 3 smaller than reported in Ref. [8].

The impact of the present results is further illustrated in Table IV, where the MACS values are compared with those of Nakagawa *et al.* [30] (which are based on Ref. [8]), for different temperatures and for different upper energy limits, that is, considering only the contribution of prominent resonances below 7 keV, the resonances below 40 keV investigated in this work, and all resonances in the entire relevant energy range including the information above 40 keV from evaluated data [14,30]. The respective contributions to the MACS at the relevant values of  $kT$  confirm that the results of this work represent an essential part of the MACS at the stellar environments characterized by  $kT = 8$  and 23 keV.

The contributions calculated with the present data are 20% to 25% lower than the MACSs obtained with the evaluated data from the JENDL library [30]. Therefore, the evaluated

TABLE III. Capture kernels of the most prominent resonances and their relative contributions to the Maxwellian averaged cross sections.

$E_r$ (keV)	Kernel (eV)		Relative contribution (%)		
	This work	Ref. [8]	$kT = 8$ keV	$kT = 23$ keV	$kT = 30$ keV
2.7	0.115	0.171	6.5	2.0	1.5
4.1	0.460	0.57	21.7	8.1	5.7
5.0	0.142	0.159	6.0	2.4	1.7
6.6	0.363	0.49	12.5	5.7	4.1
6.8	0.132	0.37	4.4	2.1	1.5

data [30], which were used above 40 keV to complement the present results, have been scaled by a factor of 0.8. Concerning the definition of errors associated with the MACS, an uncertainty of 10% was considered for the contribution given by the evaluation.

The MACS derived from the experimental data in Ref. [8] are somewhat confusing. Although the JENDL evaluation [30] was obtained from these results, the MACS values in Table IV are clearly discrepant [36]. Moreover, the same experimental data [8] were used in another publication by the same authors [37], where the MACS at 30 keV was stated to be 51 instead of the 34 mb in Ref. [8], and both values were subsequently scaled by a common correction factor [38], to 50 and 33 mb, respectively.

In a previous publication [39] we quoted a preliminary value of  $29 \pm 2$  mb for the MACS at 30 keV; the difference from the present value is related to a better treatment of the complementary part, above 40 keV.

The final MACSs are compared with previous data in Fig. 5. In this figure the solid and dashed lines represent evaluations based on the data from Ref. [8]; the solid line represents the MACSs calculated on the basis of the evaluated data in the JENDL library [30,36], and the dashed line refers to the MACS compilation of Bao *et al.* [4]. The present data agree with Ref. [4] (and disagree with Ref. [30]) at low temperatures; however, it must be noted that the agreement with Ref. [4] progressively vanishes toward higher temperatures. In this

TABLE IV. Maxwellian averaged cross sections (MACSs; mb) calculated for different thermal energies and upper integration limits, compared with those extracted from the data in Ref. [30].

Contribution to MACS	$kT = 8$ keV	$kT = 23$ keV	$kT = 30$ keV
$E_n \leq 7$ keV			
Ref. [30]	$74 \pm 8$	$14 \pm 1.5$	$9.3 \pm 0.9$
This work	$58 \pm 3$	$12 \pm 0.6$	$7.5 \pm 0.4$
$E_n \leq 40$ keV			
Ref. [30]	$115 \pm 11$	$39 \pm 4$	$28 \pm 3$
This work	$95 \pm 5$	$33 \pm 1.6$	$24 \pm 1.2$
Full range			
Ref. [4]	–	–	$33 \pm 4$
Ref. [30]	$117 \pm 12$	$52 \pm 5$	$46 \pm 5$
This work	$97 \pm 5$	$44 \pm 3$	$38 \pm 3$

context, we remind that the uncertainties of the present results are partly related to the assumption used for the extrapolation above 40 keV. The weight of the extrapolation, and consequently the uncertainty in the MACS, increases with increasing temperature, reaching approximately 10% at  $kT = 80$  keV. A reduction of the overall uncertainty for high temperatures could eventually be achieved by new, accurate measurements at energies above 40 keV. Moreover, the MACS reported in this work should be corrected for the contribution of the direct capture process. Preliminary calculations indicate that such a contribution is small at low temperatures but becomes important with increasing temperatures, reaching about 8% at 30 keV. A more comprehensive analysis of the direct capture contribution, for this as well as for other Zr isotopes, will be the subject of a forthcoming publication [40].

The impact of the new MACS values on the  $s$ -process yield of  $^{92}\text{Zr}$  was calculated with the stellar model for thermally

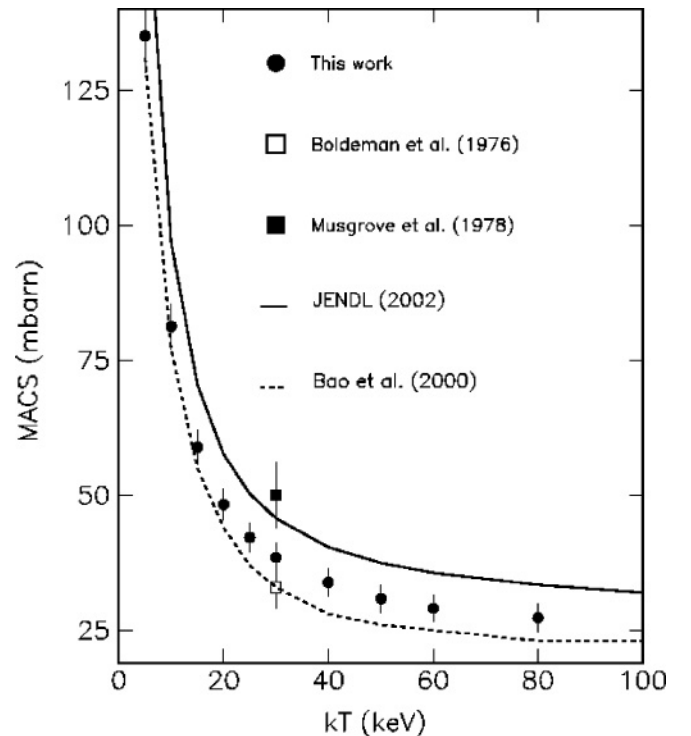


FIG. 5. Comparison of present MACSs (filled circles) with values from Refs. [4], [8], [30], and [37].

pulsing low-mass AGB stars [6,33]. It turned out that the MACSs of this work translate into a 3% reduction of the  $s$ -process contribution to the solar abundance of  $^{92}\text{Zr}$  compared to the solution obtained with the previously recommended data in Ref. [4]. This difference is significantly smaller than one would expect by simply scaling the product of  $\langle\sigma\rangle N_s$  that characterizes the reaction flow in the classical  $s$ -process approach [41], thus reflecting the more dynamic situation described by the stellar model.

As expected from the nearly saturated reaction flow in thermally pulsing low-mass AGB stars, there are practically no propagation effects concerning the abundances of the subsequent isotopes in the reaction path apart from the change in the  $^{92}\text{Zr}$  abundance itself. The only exception is  $^{93}\text{Nb}$ , which is enhanced by 3% via the decay of the immediate neighbor  $^{93}\text{Zr}$ . Although these changes are small and comparable to the 6% uncertainty in the solar Zr abundance [42], the corresponding solar  $r$  abundances obtained as the difference between the solar value and the  $s$  component,  $N_r = N_\odot - N_s$ , is about 40% higher for  $A = 92$  (from 6.5 to 9.2) and one-third lower for  $A = 93$  (from 14.6 to 10.0). While the uncertainty of the important  $s$ -process abundance of  $^{92}\text{Zr}$  was significantly improved, from 14% in Ref. [6] to 8%, the related small  $r$  component still carries an uncertainty of 100%. Nevertheless, the revised  $r$ -abundance values fit better to the expected smoothness of the  $r$  distribution [6].

## VIII. CONCLUSIONS

The  $(n, \gamma)$  cross section of  $^{92}\text{Zr}$  has been measured over a wide range of neutron energies using the innovative features of the n\_TOF facility at CERN. Resonance parameters were determined for 44 resonances in the neutron energy range up to 40 keV.

The capture kernels of the analyzed resonances are  $\approx 20\%$  smaller than reported previously. The low neutron-induced background that was obtained with the optimized experimental setup and the extremely small duty factor of the n\_TOF facility contributed to a significant improvement in the small neutron capture cross section of  $^{92}\text{Zr}$ .

Based on the present results, MACSs for  $s$ -process studies of stellar nucleosynthesis were obtained and may be used to improve the recommended data in Ref. [4]. The cross section determined in this work leads to a reduction in the  $s$  component of  $^{92}\text{Zr}$ . The corresponding increase in the  $r$ -process contribution results in a better agreement with the smooth distribution of the solar  $r$ -process abundances [6].

## ACKNOWLEDGMENTS

This work was supported by the EC under Contract No. FIKW-CT-2000-00107 and by the funding agencies of the participating institutes.

- 
- [1] G. Wallerstein *et al.*, *Rev. Mod. Phys.* **69**, 995 (1997).  
 [2] E. M. Burbidge, G. R. Burbidge, W. A. Fowler, and F. Hoyle, *Rev. Mod. Phys.* **29**, 547 (1957).  
 [3] M. Lugaro, F. Herwig, J. C. Lattanzio, R. Gallino, and O. Straniero, *Astrophys. J.* **586**, 1305 (2003).  
 [4] Z. Y. Bao, H. Beer, F. Käppeler, F. Voss, K. Wisshak, and T. Rauscher, *At. Data Nucl. Data Tables* **76**, 70 (2000).  
 [5] R. L. Macklin and J. H. Gibbons, *Phys. Rev.* **159**, 1007 (1967).  
 [6] C. Arlandini, F. Käppeler, K. Wisshak, R. Gallino, M. Lugaro, M. Busso, and O. Straniero, *Astrophys. J.* **525**, 886 (1999).  
 [7] J. F. Minster and C. J. Allegre, *Geochim. Cosmochim. Acta* **46**, 565 (1982).  
 [8] J. W. Boldeman, A. R. de L. Musgrove, B. J. Allen, J. A. Harvey, and R. L. Macklin, *Nucl. Phys. A* **269**, 31 (1976).  
 [9] Z. M. Bartolome, R. W. Hockenbury, W. R. Moyer, J. R. Tatarczuk, and R. C. Block, *Nucl. Sci. Eng.* **37**, 137 (1969).  
 [10] W. M. Good and H. Kim, *Phys. Rev.* **165**, 1329 (1968).  
 [11] S. S. Moskalev, H. V. Muradian, and Yu. V. Adamchuk, *Nucl. Phys.* **53**, 667 (1964).  
 [12] K. Ohgama, M. Igashira, and T. Ohsaki, *J. Nucl. Sci. Technol.* **42**, 333 (2005).  
 [13] S. F. Mughabghab, *Atlas of Neutron Resonances, Resonance Parameters and Thermal Cross Sections Z = 1–100* (Elsevier Science, Amsterdam, 2006).  
 [14] For results compiled in evaluated nuclear data libraries see, e.g., International Atomic Energy Agency (IAEA), [[www-nds.iaea.org](http://www-nds.iaea.org)], or OECD Nuclear Energy Agency, [[www.nea.fr/html/dbdata/](http://www.nea.fr/html/dbdata/)].  
 [15] G. Tagliente *et al.*, *Phys. Rev. C* **77**, 035802 (2008).  
 [16] G. Tagliente *et al.*, *Phys. Rev. C* **78**, 045804 (2008).  
 [17] U. Abbondanno *et al.*, CERN n\_TOF facility: Performance report, CERN-SL-2002-053 ECT (2003).  
 [18] S. Marrone *et al.*, *Nucl. Instrum. Methods A* **517**, 389 (2004).  
 [19] R. Plag, M. Heil, F. Käppeler, P. Pavlopoulos, R. Reifarth, and K. Wisshak, *Nucl. Instrum. Methods A* **496**, 425 (2003).  
 [20] S. Marrone *et al.*, *Phys. Rev. C* **73**, 034604 (2006).  
 [21] U. Abbondanno *et al.*, *Nucl. Instrum. Methods A* **538**, 692 (2005).  
 [22] F. Corvi, G. Fioni, F. Gasperini, and P. B. Smith, *Nucl. Sci. Eng.* **107**, 272 (1991).  
 [23] J. N. Wilson, B. Haas, S. Boyer, D. Dassie, G. Barreau, M. Aiche, S. Czajkowski, C. Grosjean, and A. Guiral, *Nucl. Instrum. Methods A* **511**, 388 (2003).  
 [24] U. Abbondanno *et al.*, *Nucl. Instrum. Methods A* **521**, 454 (2004).  
 [25] R. L. Macklin and J. Halperin, *Phys. Rev. C* **14**, 1389 (1976).  
 [26] C. Borcea *et al.*, *Nucl. Instrum. Methods A* **513**, 524 (2003).  
 [27] G. Aerts *et al.*, *Phys. Rev. C* **73**, 054610 (2006).  
 [28] G. Lorusso *et al.*, *Nucl. Instrum. Methods A* **532**, 622 (2004).  
 [29] N. M. Larson, *Updated Users' Guide for SAMMY: Multilevel R-Matrix Fits to Neutron Data Using Bayes' Equations*, Report ORNL/TM-9179/R7 (Oak Ridge National Laboratory, Oak Ridge, TN, 2006).  
 [30] T. Nakagawa, S. Chiba, T. Hayakawa, and T. Kajino, *At. Data Nucl. Data Tables* **91**, 77 (2005); K. Shibata *et al.*, *J. Nucl. Sci. Technol.* **39**, 1125 (2002).

- [31] R. L. Macklin and B. J. Allen, *Nucl. Instrum. Methods* **91**, 565 (1971).
- [32] C. M. Raiteri, R. Gallino, M. Busso, D. Neuberger, and F. Käppeler, *Astrophys. J.* **419**, 207 (1993).
- [33] R. Gallino, C. Arlandini, M. Busso, M. Lugaro, C. Travaglio, O. Straniero, A. Chieffi, and M. Limongi, *Astrophys. J.* **497**, 388 (1998).
- [34] M. Lugaro, F. Herwig, J. C. Lattanzio, R. Gallino, and O. Straniero, *Astrophys. J.* **586**, 1305 (2003).
- [35] I. Dillmann, M. Heil, F. Käppeler, R. Plag, T. Rauscher, and F.-K. Thielemann, in *Capture Gamma-Ray Spectroscopy and Related Topics*, AIP Conference Series 819, edited by A. Woehr and A. Aprahamian (AIP, New York, 2005), p. 123 (see also [<http://www.kadonis.org>]).
- [36] [[www.wndc.jaea.go.jp/nakagawa/MaxwAv/Figs/Zr092.pdf](http://www.wndc.jaea.go.jp/nakagawa/MaxwAv/Figs/Zr092.pdf)].
- [37] A. de L. Musgrove, B. J. Allen, J. W. Boldeman, and R. L. Macklin, in *Neutron Physics and Nuclear Data for Reactors and Other Applied Purposes* (OECD, Paris, 1978), p. 449.
- [38] B. J. Allen, J. W. Boldeman, and R. L. Macklin, *Nucl. Sci. Eng.* **82**, 230 (1982).
- [39] G. Tagliente *et al.*, *Nuclei in the Cosmos-IX, Proceedings of Science, SISSA, Trieste*, edited by A. Mengoni *et al.*, available at: [[http://pos.sissa.it/archive/conferences/028/227/NIC-IX\\_227.pdf](http://pos.sissa.it/archive/conferences/028/227/NIC-IX_227.pdf)].
- [40] A. Mengoni *et al.*, in preparation (2010).
- [41] P. A. Seeger, W. A. Fowler, and D. D. Clayton, *Astrophys. J. Suppl.* **11**, 121 (1965).
- [42] E. Anders and N. Grevesse, *Geochim. Cosmochim. Acta* **53**, 197 (1989).